

# Highly Efficient In Vivo Targeting of the Pulmonary Endothelium Using Novel Modifications of Polyethylenimine: An Importance of Charge

Andrew W. Dunn, Vladimir V. Kalinichenko, and Donglu Shi\*

Pulmonary vascular disease encompasses a wide range of serious afflictions with important clinical implications. There is critical need for the development of efficient, nonviral gene therapy delivery systems. Here, a promising avenue to overcome critical issues in efficient cell targeting within the lung via a uniquely designed nanosystem is reported. Polyplexes are created by functionalizing hyperbranched polyethylenimine (PEI) with biological fatty acids and carboxylate-terminated poly(ethylene glycol) (PEG) through a one-pot 1-ethyl-3-(3-dimethylaminopropyl)carbodiimide hydrochloride/*N*-hydroxysuccinimide reaction. Following intravenous injection, polyplexes show an exceptionally high specificity to the pulmonary microvascular endothelium, allowing for the successful delivery of stabilized enhanced green fluorescent protein (eGFP) expressing messenger ribonucleic acid (mRNA). It is further shown, quantitatively, that positive surface charge is the main mechanism behind such high targeting efficiency for these polyplexes. Live in vivo imaging, flow cytometry of single cell suspensions, and confocal microscopy are used to demonstrate that positive polyplexes are enriched in the lung tissue and disseminated in 85–90% of the alveolar capillary endothelium, whilst being sparse in large vessels. Charge modification, achieved through poly(acrylic acid) or heparin coating, drives a highly significant reduction in both targeting percentage and targeting strength, highlighting the importance of specific surface charge, derived from chemical formulation, for efficient targeting of the pulmonary microvascular endothelium.

## 1. Introduction

Pulmonary vascular disease (PVD) encompasses a wide range of pediatric and adult pulmonary disorders, such as pulmonary

A. W. Dunn, Prof. D. Shi  
The Materials Science and Engineering Program  
Department of Mechanical and Materials Engineering  
College of Engineering and Applied Sciences  
University of Cincinnati  
Cincinnati, OH 45221, USA  
E-mail: donglu.shi@uc.edu

Dr. V. V. Kalinichenko  
Center for Lung Regenerative Medicine  
Division of Pulmonary Biology and the Perinatal Institute  
Cincinnati Children's Hospital Research Foundation  
Cincinnati, OH 45229, USA

 The ORCID identification number(s) for the author(s) of this article can be found under <https://doi.org/10.1002/adhm.201800876>.

DOI: 10.1002/adhm.201800876

hypertension, alveolar capillary dysplasia, and various arterial, venous, and lymphatic malformations.<sup>[1,2]</sup> PVD is associated with poor prognosis in patients with bronchopulmonary dysplasia, a severe respiratory disorder of infants.<sup>[3,4]</sup> Gene therapy by adenovirus vectors has shown to ameliorate pulmonary hypertension, and stimulate endothelial repair after chronic lung injury.<sup>[5,6]</sup> However, major detractions of viral vectors to clinical translation include a potent ability to elicit a significant immune response and potential random integration genome integration based on vector type.<sup>[7–9]</sup> Efficient, nonviral delivery systems specifically targeting the pulmonary endothelium are therefore critically needed to treat PVD.

Polyethylenimine (PEI) has been used successfully for nonviral transfections in part owing to its high buffer capacity, aiding in the escape of intracellular compartmentalization.<sup>[10,11]</sup> High molecular weight, branched PEI has been shown to be more efficient than low molecular weight PEI and more resistant to aggregation in salt solutions than linear PEI.<sup>[12–14]</sup> However, a drawback of higher molecular weight PEI is the observed increase in cytotoxicity jux-

taposed with lower molecular weight variants.<sup>[14]</sup> Recent research has seen the modification of low molecular weight PEI for reduced toxicity and improved transfection efficiency.<sup>[15]</sup> Modification of PEI and other amine dense polymers, such as polypropylenimine, has been done through ring opening synthesis,<sup>[16–18]</sup> amidation by activated carboxylate groups,<sup>[19–21]</sup> through the Schotten–Baumann reaction using carboxylic acid chlorides,<sup>[22]</sup> and by Michael addition.<sup>[23–25]</sup> The grafting of small alkane tails, aryl, and hydrophobic groups induces amphiphilic behavior, allowing for the formation of nanocolloids in solution.<sup>[16,23,26–28]</sup> This modification essentially creates a pseudolipid which spontaneously forms micellar structures in aqueous solutions.

Colloidal stability of these lipid-like micelles has been shown to be improved through the inclusion of cholesterol, with an observed decrease in colloidal size and improved efficacy.<sup>[17,29,30]</sup> Further inclusion of poly(ethylene glycol) (PEG) has been shown to modify serum interaction and reduce opsonization, thereby increasing circulation time.<sup>[31–34]</sup> These strategies have been focused on therapeutic delivery of RNA or DNA.<sup>[17,32,35,36]</sup>

Cationic formulations created in this manner have shown an ability to target the endothelial cells in vivo post intravenous (I.V.) delivery.<sup>[17]</sup> While mediation of nanoparticle surface charge on physiological interactions, such as biodistribution and cellular association, has been investigated and positively charged particles on the whole organ level have been shown targeting the lung,<sup>[37,38]</sup> the effects of specific surface charge on cell-type targeting and nanoparticle distribution within the lung are not well known.

Research on polymeric-based gene delivery has commonly focused on local injections to a target region. This delivery strategy is not widely applicable for translational application, especially in the case of large target areas requiring widespread dissemination. Here, we report the development and characterization of 600 Da, 1800 Da, and 10 kDa, branched PEI-based nanoparticles, possessing hydrodynamic size and surface charge near 120 nm and 24 mV, respectively, capable of targeting the pulmonary endothelium in a charge-dependent manner with exceptionally high efficiency for the delivery of nucleic acids. Furthermore, nanoparticle dissemination within the lung is shown to be preferentially associated with the microvascular network, a key target for therapy; this property is not commonly presented in characterization of charged-based targeting.

## 2. Results

### 2.1. Synthesis and Characterization

A schematic diagram of the synthesis method is shown in Figure S1 (Supporting Information). This scheme was further used for the functionalization of oleic acid (OA) to 2 kDa carboxylate-terminated PEG (PEG-OA). 600 Da PEI (PEI<sub>600</sub>) was functionalized with myristic acid (MA) in a 1:5 molar ratio (PEI<sub>600</sub>-MA<sub>5</sub>). Linoleic acid (LinA) and 2 kDa PEG was conjugated to 1.8 and 10 kDa PEI in 1:5:0.3 and 1:15:3 molar ratios, respectively, to create PEI<sub>1800</sub>-LinA<sub>5</sub>-PEG<sub>0.3</sub> and PEI<sub>10k</sub>-LinA<sub>15</sub>-PEG<sub>3.0</sub>. Functionalized polymers were dialyzed against water, extracted in diethyl ether, and lyophilized. PEI<sub>600</sub>-MA<sub>5</sub> was combined with cholesterol (Cho) and PEG-OA through microfluidic mixing for size optimization.

Attenuated total reflectance Fourier transform infrared (ATR-FTIR) analysis confirmed successful amidation by appearance of an amide carbonyl  $\nu = 1650 \text{ cm}^{-1}$  (s) in the conjugated polymers (Figure 1A and Figures S2 and S3 (Supporting Information)). PEG,  $\nu = 1100 \text{ cm}^{-1}$  (s; C–O), and the sp<sup>2</sup> carbon bonds of linoleic acid  $\nu = 3050 \text{ cm}^{-1}$  (s; C=C) were observed in the PEI<sub>10k</sub>-LinA<sub>15</sub>-PEG<sub>3.0</sub> and PEI<sub>1800</sub>-LinA<sub>5</sub>-PEG<sub>0.3</sub> spectrum (Figure 1A and Figure S2 (Supporting Information)) as well as by <sup>1</sup>H NMR in CDCl<sub>3</sub> (Figure 1B). Table 1 shows the calculated degree of conjugation (DoC) for PEI<sub>600</sub>, PEI<sub>1800</sub>, and PEI<sub>10k</sub>. Conjugation is close to theoretical ratios for lower ratios used during PEI<sub>600</sub> conjugation but begin to drift when using higher molecular weights.

Gel electrophoresis was used to determine the onset of stabilization. The onset of stabilization was taken to be the w/w which fully restricted DNA migration (Figure 1C). Size quantifications for PEI<sub>600</sub>-MA<sub>5</sub>, PEI<sub>1800</sub>-LinA<sub>5</sub>-PEG<sub>0.3</sub>, and PEI<sub>10k</sub>-LinA<sub>15</sub>-PEG<sub>3.0</sub> were done at w/w = 21, 25, and 15,

respectively, in normal glucose and Figure 1D shows the monodisperse characteristics for the hydrodynamic diameter distribution of PEI<sub>10k</sub>-LinA<sub>15</sub>-PEG<sub>3.0</sub> polyplexes. The size-optimized formulation of PEI<sub>600</sub>-MA<sub>5</sub>:PEG-OA:Cho at w/w = 24 was created using a mass ratio of 100:11.1:11.1 (Table S1, Supporting Information). All three formulations showed colloidal stability with no significant differences found between colloidal sizes at 7 days postformulation compared to initial measurements (Figure S4 and Table S2, Supporting Information).

### 2.2. In Vivo Targeting of Cationic Polyplexes

Initial in vivo screening revealed a targeting dependence on chemical formulation (Figure S6, Supporting Information). A zeta potential near +40 mV was associated with reduced targeting efficiency of the endothelial population compared to formulations near +15 mV. Polyplexes were therefore created to possess a final positive zeta potential of less than +40 mV with a target hydrodynamic diameter of less than 200 nm. Functionalized PEI was mixed with 40  $\mu\text{g}$  of purified plasmid DNA at mass ratios w/w dependent upon the onset of stabilization as quantified by gel electrophoresis and diluted in normal glucose. Polyplex sizes were within the useful range for in vivo application<sup>[39]</sup> and chosen zeta potential range (Table 2). Targeting efficiency of DyLight 650-labeled polyplexes was determined 24 h post tail vein injection in healthy, adult male, wild-type C57BL6/J mice by flow cytometry. Cell populations examined were gated as live singlet CD45+ CD31– (hematopoietic), CD31+ CD326– CD45– (endothelial), CD326+ CD31– CD45– (epithelial), and CD45– CD31– CD326– (lineage negative, cell population mostly containing fibroblasts and pericytes). Figure 2A shows a representation of the gated populations with a full gating strategy presented in Figure S5 (Supporting Information). Figure 2B shows the fluorescent histogram for PEI<sub>10k</sub>-LinA<sub>15</sub>-PEG<sub>3.0</sub> against the fluorescence minus one (FMO) control. A comparison of targeting efficiencies ( $n = 3$ ) is presented in Figure 2C. Stabilized enhanced green fluorescent protein (eGFP) RNA complexed with PEI<sub>10k</sub>-LinA<sub>15</sub>-PEG<sub>3.0</sub> was delivered intravenously in normal glucose; the median fluorescent intensity (MFI) from endothelial cells isolated 24 h postinjection was quantified by flow cytometry and was found to be significantly higher than control mice ( $p < 0.05$ ,  $n = 5$ ) (Figure 2C inset).

### 2.3. Immunofluorescence of Cationic Polyplexes

The distribution of DyLight 650-tagged PEI<sub>10k</sub>-LinA<sub>15</sub>-PEG<sub>3.0</sub> nanoparticles in the lung tissue was investigated using 10  $\mu\text{m}$  frozen lung sections harvested from healthy adult male, wild-type C57BL6/J mice 24 h post tail vein injection. Sections were stained with Hoechst 33342 (nuclear stain), platelet endothelial cell adhesion molecule (PECAM1, CD31), and alpha smooth muscle actin ( $\alpha\text{SMA}$ ) for visualization of microvasculature and large vessels. Confocal images of stained sections show that nanoparticles (NPs) were highly disseminated throughout the pulmonary microvasculature, as shown by colocalization of DyLight with PECAM1 (Figure 3A–A" and Figure S7

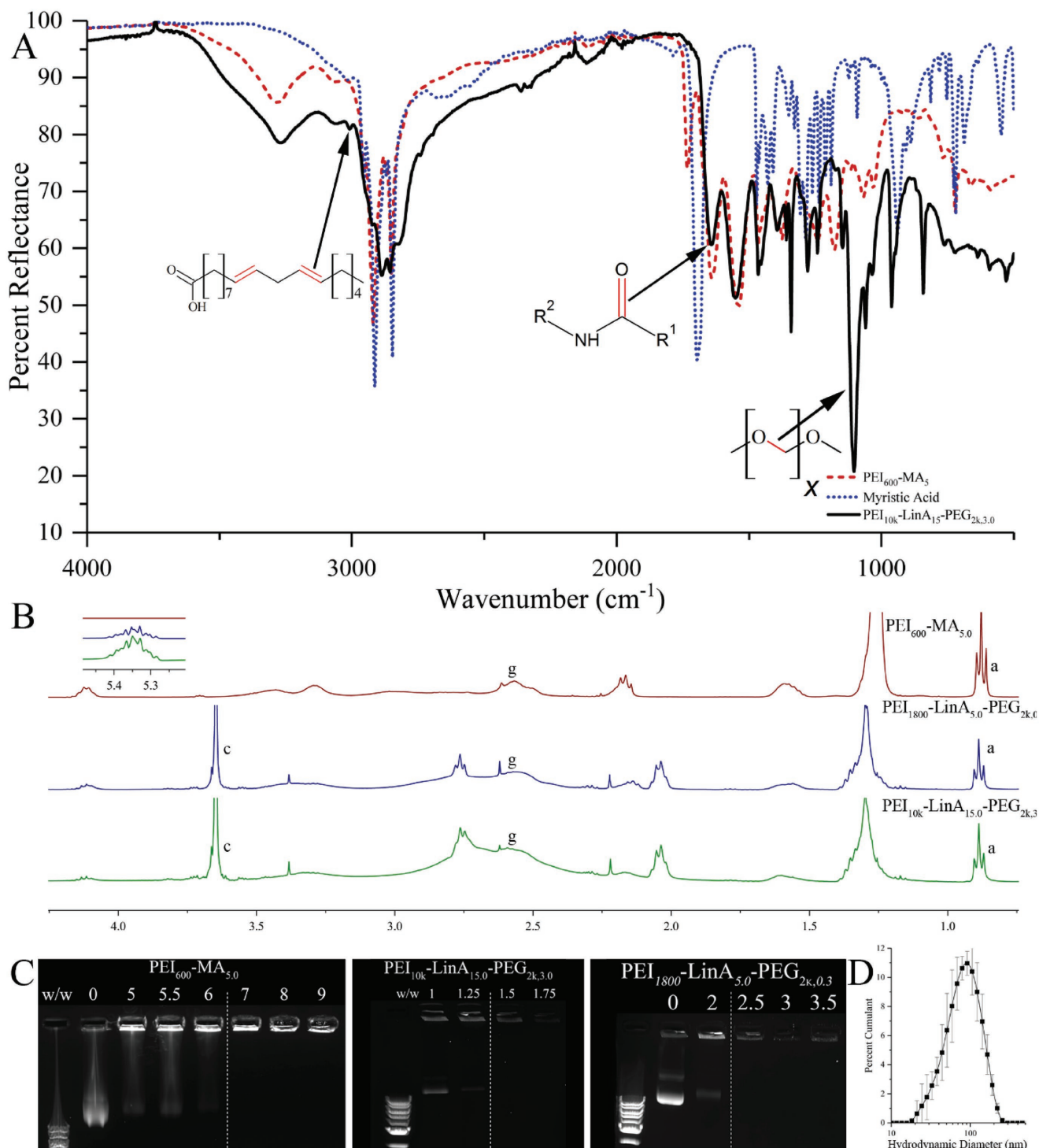


**Figure 1.** A) atr-FTIR spectrum of myristic acid (dotted), PEI<sub>600</sub>-MA<sub>5</sub> (dashed), and PEI<sub>10k</sub>-LinA<sub>15</sub>-PEG<sub>3,0</sub> (solid), showing amidation after conjugation as well as inclusion of PEG and linoleic acid on to PEI<sub>10k</sub>. B) <sup>1</sup>H NMR spectrum of conjugated polymers. C) Gel electrophoresis analysis of CMV-empty plasmids bound to conjugated PEI at varying mass ratios of polymer:DNA w/w. D) Hydrodynamic size distribution of PEI<sub>10k</sub>-LinA<sub>15</sub>-PEG<sub>3,0</sub> in normal glucose used for I.V. injection.

(Supporting Information)). NPs within the lumen of larger vessels were sparse (Figure 3B–B'', 3C–C''). This is likely a result of hemodynamic differences between large vessels and capillary beds. Figure 3C'' shows the NPs found within the lumen of large vessels colocalized with PECAM1.

#### 2.4. Zeta-Potential Switching

To further investigate the mechanism behind charged-based, nonaffinity targeting within the lung, the zeta (surface) potential of the cationic polyplex with the highest targeting affinity

**Table 1.** DoC for fatty acid and PEG<sub>2k</sub>-conjugated PEI determined by <sup>1</sup>H NMR.

	Fatty acid	PEG <sub>2k</sub>
PEI <sub>600</sub> -MA <sub>5</sub>	5.2 ± 0.7	
PEI <sub>1800</sub> -LinA <sub>5</sub> -PEG <sub>0.3</sub>	6.5 ± 0.8	0.39 ± 0.03
PEI <sub>10k</sub> -LinA <sub>15</sub> -PEG <sub>3.0</sub>	20.7 ± 2	1.95 ± 0.15

(PEI<sub>10k</sub>-LinA<sub>15</sub>-PEG<sub>3.0</sub>, Figure 2) for the lung endothelium was switched by coating with poly(acrylic acid) (PAA) through ionic interaction. Two mass ratios of PEI:DNA were used for sizing and zeta-potential analysis post PAA coating to investigate the possibility of using a standard mass ratio of PAA:PEI regardless of the w/w ratio used (Figure 4). In both the cases, for the mass ratios of PAA:PEI (0%, 10%, 25%, 50%) used, at least 25% was required to switch the zeta potential while maintaining a nonsignificantly different hydrodynamic diameter. A further coating of 50% significantly, negatively shifted the zeta potential while not significantly effecting hydrodynamic size for both w/w ratios used. A PAA coating of 10% by mass led to a relatively slight negative shift in zeta potential, however with the zeta potential remaining positive, coupled with a significant increase in hydrodynamic diameter (Figure 4 and Table 3). PAA coating following polyplex formation therefore induced zeta-potential switching without impacting the hydrodynamic diameter, thereby allowing for investigation on the importance of charge on endothelial targeting within the lung irrespective of initial polyplex size.

## 2.5. In Vivo Targeting of Negatively Charged Polyplexes

For investigation behind the mechanism governing such robust targeting observed with positively charged polyplexes, negatively charged polyplexes were formulated by coating of negatively charged polymers post polyplex formation. PAA-coated PEI<sub>10k</sub>-LinA<sub>15</sub>-PEG<sub>3.0</sub> was used to investigate the dependence of endothelial targeting within the lung on initial zeta potential prior to I.V. injection. The gating strategy shown in Figure 2A was repeated to categorize the four lineages 24 h postdelivery of negatively or positively charged DyLight 650-labeled polyplexes in healthy, adult male, wild-type C57BL6/J mice by flow cytometry. Juxtaposition of cells isolated from mice given negatively charged polyplexes (black filled histogram) and mice given positively charged polyplexes (blue dashed histogram) show a robust loss in both percent targeting and strength of targeting, as quantified by MFI, for the negative polyplexes within the endothelial lineage (Figure 5A). These shifts in targeting corresponded to a significant reduction in both percent

**Table 2.** Hydrodynamic sizes and zeta potentials of polyplexes in normal glucose.

	w/w	Z-average [d.nm]	Zeta potential [mV]
PEI <sub>600</sub> -MA <sub>5</sub> /PEG-OA/Cho	21	123 ± 49	24.0 ± 5.1
PEI <sub>1800</sub> -LinA <sub>5</sub> -PEG <sub>0.3</sub>	25	142 ± 66	22.2 ± 5.4
PEI <sub>10k</sub> -LiA <sub>15</sub> -PEG <sub>3.0</sub>	15	107 ± 56	23.7 ± 7.4

targeting (15.0 ± 1.5% (–) vs 91.8 ± 1.3% (+), *p* < 0.001) and MFI as standardized using the FMO control (2.9 ± 0.2% (–) vs 406 ± 122% (+), *p* < 0.01) (Figure 5B). Furthermore, a significant reduction in MFI within the hematopoietic and lineage negative populations was also observed (*p* < 0.01) with no significant differences found within the epithelial lineage.

Immunofluorescent imaging of frozen lung sections corroborated results presented by fluorescent-activated cell sorting (FACS) analysis (Figure 5C). Nanoparticle fluorescence from negative polyplexes was not observed within the microvasculature when juxtaposed with fluorescence acquired from positive polyplexes when imaged under equivalent parameters (Figure 5Ca–c). Fluorescence from negative polyplexes was absent from within the lumen of large vessels (Figure 5Ca',b'), similar to positive polyplexes. Positive polyplex association within the lumen of distal vessels and targeting of the distal microvasculature was also found. (Figure 5Cc' and Figure S8 (Supporting Information)). Likewise, this reduction in targeting was further observed following I.V. delivery of negatively charged polyplexes established through heparin coating (Figure S9, Supporting Information).

## 2.6. Biodistribution

Richardson–Lucy deconvolution was performed on a Z-stack image of lung microvasculature. Figure 6A shows a 3D maximum intensity projection of a deconvoluted Z-stack showing Hoechst nuclear staining (blue), PECAM1 (green), PEI<sub>10k</sub>-LinA<sub>15</sub>-PEG<sub>3.0</sub> (red). This maximum intensity plot was subsequently used for the automated surface plot generation in Imaris and used for determining the percentage of nanoparticle internalization (Figure 6B). The internalization, as calculated based on nanoparticle fluorescence within the PECAM1 surface stain, was found to be 63.8 ± 17.6% (Figure 6C). For investigation of possible targeting in other organ systems, live in vivo imaging was completed using an IVIS SpectrumCT. Mice were given DyLight 650-conjugated PEI<sub>10k</sub>-LinA<sub>15</sub>-PEG<sub>3.0</sub> complexed with 40 μg of plasmid DNA in normal glucose injected as a 200 μL bolus through the tail vein. An uninjected control mouse (left) was imaged simultaneously alongside an injected mouse (right) at each time point (Figure 6D). Acquisition shows dissemination throughout the mouse with maximal accumulation in regions near the lung and kidneys. Fluorescence intensity appeared static and was stable for the entirety of the study (7 days).

## 3. Discussion

In this study, we generated three novel formulations of PEI-based polyplexes that target pulmonary microvascular endothelium with high specificity. Hyperbranched PEI was easily functionalized with biological fatty acids or PEG. The conjugation of fatty acids onto PEI was completed by amidation using 1-ethyl-3-(3-dimethylaminopropyl)carbodiimide hydrochloride (EDC)/N-hydroxysuccinimide (NHS) coupling with conjugation, confirmed by atr-FTIR and <sup>1</sup>H NMR spectroscopy. For PEI<sub>600</sub>, quantification of molar degree of conjugation by <sup>1</sup>H NMR analysis was found to closely match the theoretical degree

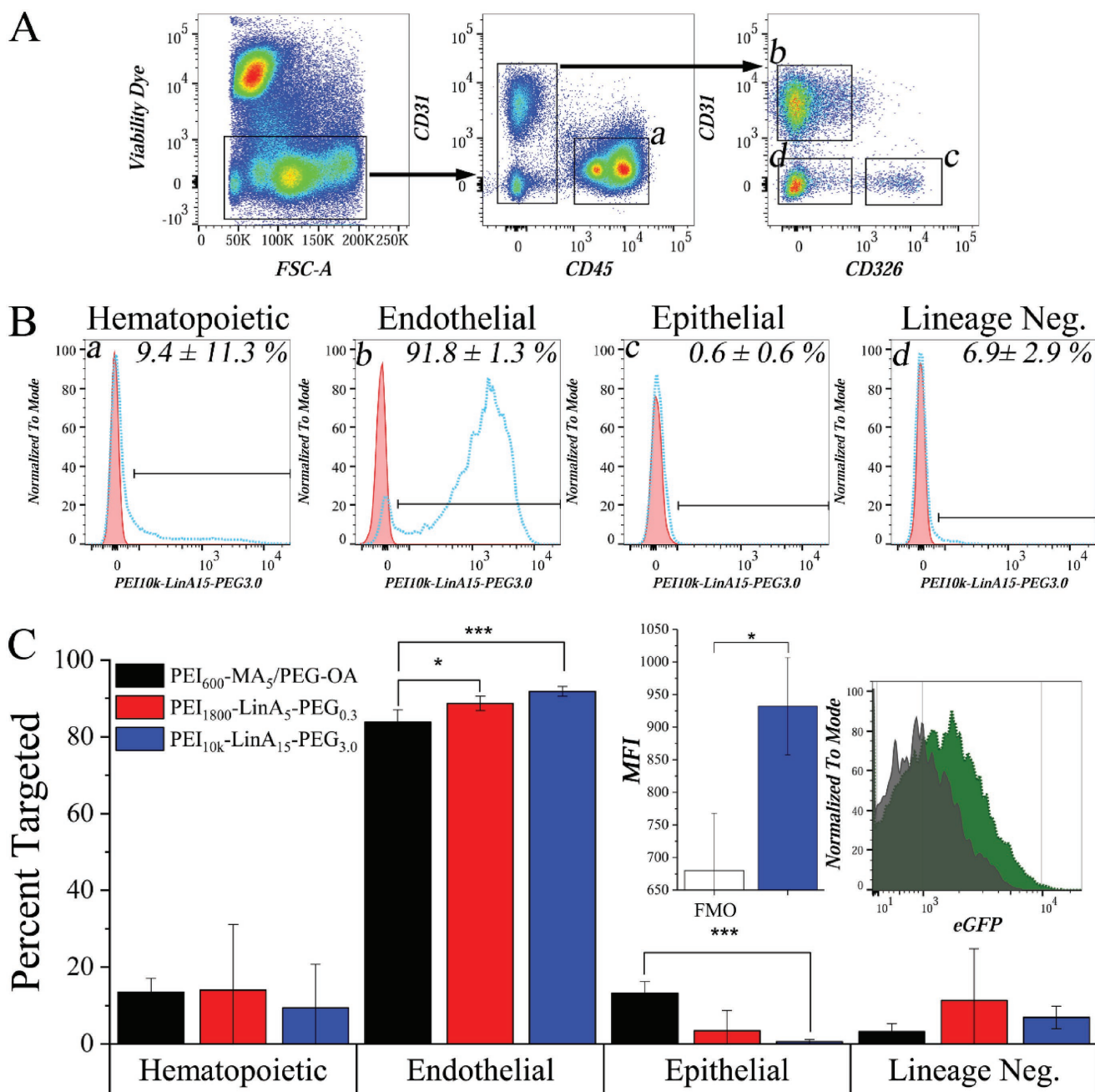


**Figure 2.** A) Gating strategy for identification of lineage populations from live singlet cells isolated from whole lung. Population (A-a) is identified as the hematopoietic population, (A-b) as the endothelial population, (A-c) as the epithelial population, and (A-d) as the lineage negative population. B) Histogram analysis of PEI<sub>10k</sub>-LinA<sub>15</sub>-PEG<sub>3.0</sub> (blue curve) targeting against the fluorescence minus one control (red curve). Numeric values represent the average  $\pm \sigma$  ( $n = 3$ ). C) Juxtaposition of lineage targeting from three novel formulations. PEI<sub>1800</sub>-LinA<sub>5</sub>-PEG<sub>0.3</sub> significantly increased endothelial targeting. PEI<sub>10k</sub>-LinA<sub>15</sub>-PEG<sub>3.0</sub> significantly increased endothelial and decreased epithelial targeting compared to PEI<sub>600</sub>-MA<sub>5</sub>-PEG-OA/Cho. (Inset) Median fluorescent intensity (MFI) analysis and fluorescent histogram of isolated endothelial populations from eGFP RNA transfected mice compared to fluorescence minus one (FMO) controls without injected eGFP RNA ( $n = 5$ ). \* ( $p < 0.05$ ), \*\*\* ( $p < 0.001$ ).

of conjugation. However, slight deviations from the theoretical degree of conjugation were observed for PEI<sub>1800</sub> and PEI<sub>10k</sub>.

High specificity is not a global trait of all PEI-based cationic nanoparticles. Specificity is strongly dependent upon grafting density and type of fatty acid used, as revealed by initial screening. This variation was found to be dependent upon colloidal properties with an initial, highly positive surface

potential correlating with reduced targeting efficiency, suggesting an applicable range of surface potentials for efficient targeting (Table S3, Supporting Information). The three specific formulations reported herein achieved 85–90% targeting of pulmonary endothelial cells selectively. While similar to formulations produced through epoxide-based conjugation of saturated alkane chains,<sup>[17]</sup> the mechanism behind such robust,

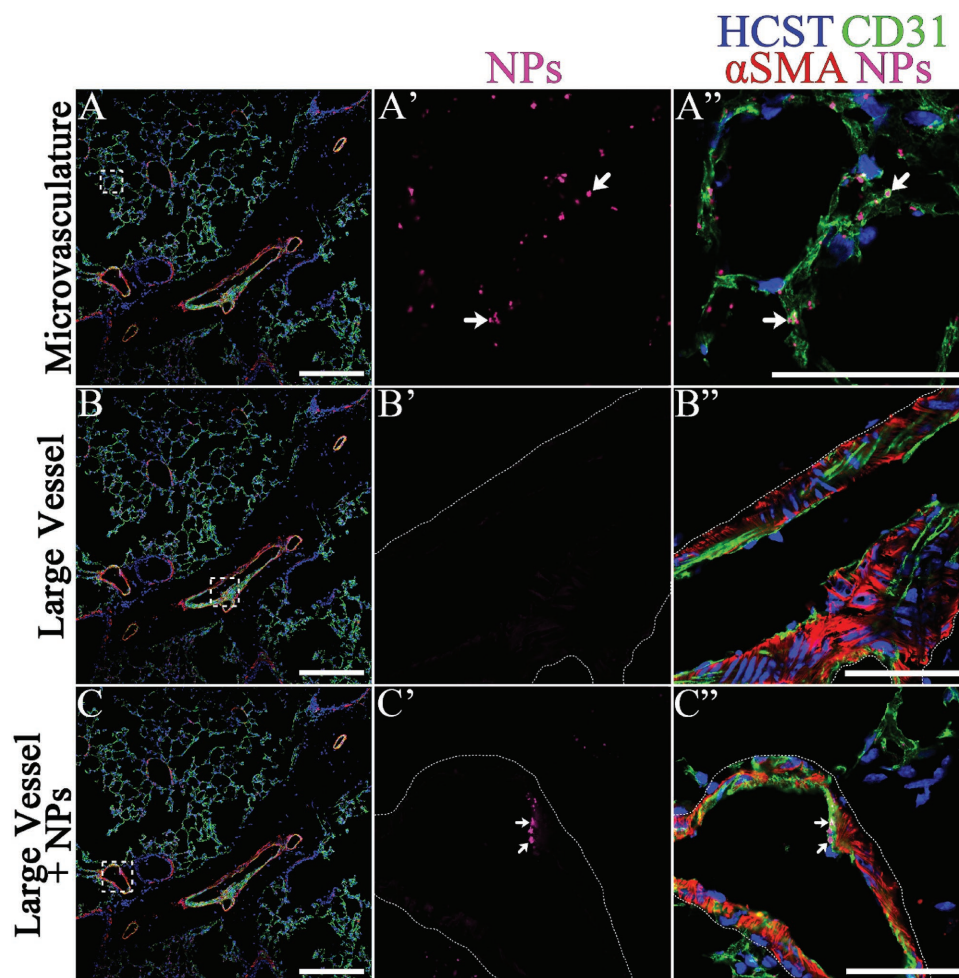


**Figure 3.** Immunofluorescence of frozen lung sections post I.V. injection of labeled PEI<sub>10k</sub>-LinA<sub>15</sub>-PEG<sub>3,0</sub>. A) Nanoparticles disseminated throughout CD31 (PECAM1) expressing cells within the microvascular network. B) Large vessels, identified by  $\alpha$ SMA staining, are associated with reduced presence of nanoparticles. C) Nanoparticles found along CD31 cells within the lumen of large vessels. A'–C') 100  $\times$  image of nanoparticle fluorescence within the respective marked areas. A''–C'') 100  $\times$  composite image within the respective marked areas. Scale bars: (A–C) 250  $\mu$ m; (A''–C'') 50  $\mu$ m.

nonaffinity targeting and characterization of distribution within the lung is not fully understood.

PEI<sub>1800</sub>-LinA<sub>5</sub>-PEG<sub>0,3</sub> was found to significantly target a larger population of endothelial cells compared to PEI<sub>600</sub>-MA<sub>5</sub>/PEG-OA/Cho ( $p < 0.05$ ) but juxtaposition of targeted hematopoietic, epithelial, and lineage negative populations revealed no significant differences. PEI<sub>10k</sub>-LinA<sub>15</sub>-PEG<sub>3,0</sub> was found to significantly target a greater population of endothelial cells compared to PEI<sub>600</sub>-MA<sub>5</sub>/PEG-OA/Cho ( $p < 0.001$ ) and a smaller population of epithelial cells ( $p < 0.001$ ); hematopoietic and lineage negative populations were not significantly different. This increase in endothelial targeting is likely a result of improved intravascular stabilization governed by the specific nanoparticle formulation, leading to improved dissemination throughout the lung microvasculature as initial colloid size and zeta potential for the three formulations do not present any significant differences at the mass ratios used for injection and is a topic for further study. Furthermore, fluorescent quantification by flow cytometry on endothelial cells isolated from mice 24 h post I.V. injection with 30  $\mu$ g of stabilized eGFP messenger ribonucleic acid (mRNA) complexed with PEI<sub>10k</sub>-LinA<sub>15</sub>-PEG<sub>3,0</sub>

showed a significant increase in MFI, indicating the ability for PEI<sub>10k</sub>-LinA<sub>15</sub>-PEG<sub>3,0</sub> to successfully deliver mRNA for translation into active protein.

As targeting was achieved through charged-based, nonaffinity binding, the importance of surface charge was investigated using the highly targeting PEI<sub>10k</sub>-LinA<sub>15</sub>-PEG<sub>3,0</sub> formulation. PAA, a polymer containing a high density of carboxylate groups, was able to reverse the surface potential while not altering polyplex size. This important decoupling of charge modification from size alteration allowed for the mechanistic investigation on the importance of initial surface charge on targeting without convolution from modifications to initial polyplex size. Flow cytometry revealed an important, significant shift in both percent targeting, ( $15.0 \pm 1.5\%$  (–) vs  $91.8 \pm 1.3\%$  (+),  $p < 0.001$ ), as well as MFI ( $2.9 \pm 0.2\%$  (–) vs  $406 \pm 122\%$  (+),  $p < 0.01$ ). This demonstrates that not only significantly fewer endothelial cells were targeted within 24 h, but the strength of targeting was further, severely reduced. Furthermore, charge modification was performed through heparin binding in a similar way to PAA. The difference being that the majority of anionic charges in heparin are derived from sulfate rather than carboxylate groups.<sup>[40]</sup> The mass ratio of

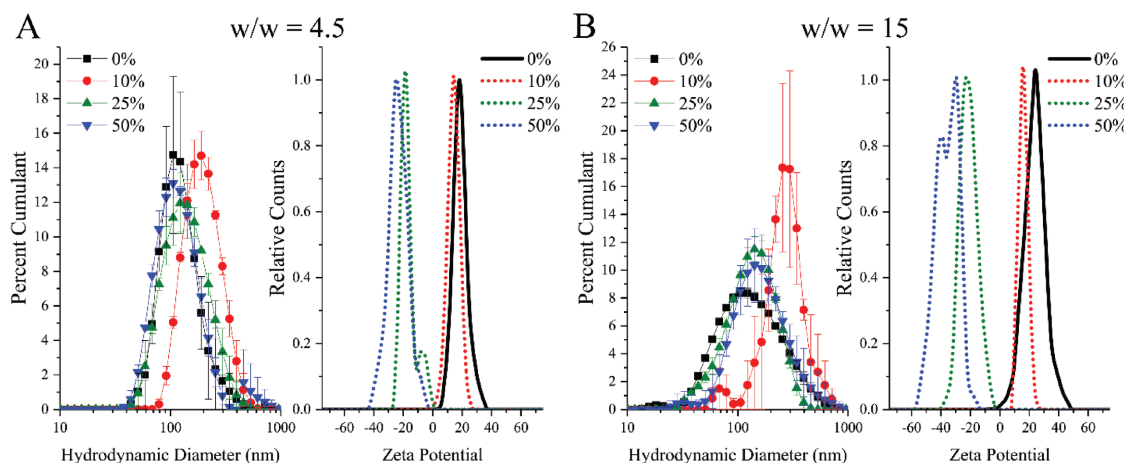


**Figure 4.** Size and zeta-potential analyses for poly(acrylic acid) (PAA)-coated PEI<sub>10k</sub>-LinA<sub>15</sub>-PEG<sub>3.0</sub> polyplexes, demonstrating charge switching using 0% (black), 10% (red), 25% (green), and 50% (blue) mass ratios of PAA relative to PEI for A) w/w = 4.5 (PEI<sub>10k</sub>:DNA) and B) w/w = 15 (PEI<sub>10k</sub>:DNA).

heparin:PEI at which a negative surface charge was measured without perturbation of polyplex size was 2:1 (200%) owing the increase in charge/molecular weight (Figure S9, Supporting Information). At 1:2 (50%), prominent aggregation was observed, whereas stable polyplexes were observed at this ratio for PAA-coated polyplexes. Immunofluorescence of the microvasculature and large vessels revealed reduced targeting similar to PAA-coated polyplexes, suggesting that the reduction in targeting from the establishment of a negative surface potential is not dependent on anionic functional group. Targeting therefore likely results from cationic polyplex interaction with the glycocalyx, a membrane-bound proteoglycan and glycoprotein cell layer upon the luminal side of vascular endothelial cells carrying a net negative charge derived from sulfated glycosaminoglycans.<sup>[41]</sup>

Nanoparticle uptake is important for successful delivery. 3D deconvolution and surface reconstruction of PECAM1 (+) endothelial cells indicated that a majority of PEI<sub>10k</sub>-LinA<sub>15</sub>-PEG<sub>3.0</sub> nanoparticles were within endothelial cells 24 h post I.V. injection by internalization of measured fluorescence. While PEI<sub>10k</sub>-LinA<sub>15</sub>-PEG<sub>3.0</sub> nanoparticle uptake is observed, it presently remains unclear as to what is the dominating mechanism as nanoparticles are known to be endocytosed by a multitude of routes, with dependencies on size and surface chemistry, including clathrin/caveolar-mediated endocytosis, phagocytosis, and macropinocytosis.<sup>[42,43]</sup> Whole body biodistribution of DyLight 650-conjugated PEI<sub>10k</sub>-LinA<sub>15</sub>-PEG<sub>3.0</sub> in adult nude mice was examined using an IVIS SpectrumCT. Live imaging revealed whole body dissemination with concentration near the lungs and kidneys; relative fluorescence distribution appeared

static and was observable for the entirety of the 7 day study. This result reflects known biodegradability and clearance properties of PEI-based nanoparticles in vivo.<sup>[44]</sup>

Previous targeting of the pulmonary endothelium for drug delivery has been achieved through antibody conjugation of therapeutic agents derived from antigen expression screening.<sup>[45–48]</sup> However, for efficient nonviral packaging of nucleic acids, cationic polymers or lipid materials are needed as the cationic nature is important for efficient, noncovalent binding of these sequences. As a result of this cationic property, small, positively charged polyplexes are inherently created when there is an excess of cationic relative to anionic charges in the complex. Efficient targeting of these polyplexes is a direct result of surface charge with a negative surface charge significantly inhibiting both percent cell targeting and targeting strength, as quantified by MFI. This suggests that surface modification of these cationic polyplexes presented herein for affinity-based targeting following formation may serve as a potent method for gene delivery while limiting vascular bed targeting due to charged-based interactions.

## 4. Conclusion

In summary, we have developed a nanoparticle system based on hyperbranched PEI of various molecular weights through a synthesis route that has allowed for a one-pot, unique conjugation scheme of biological fatty acids and PEG under green conditions. From flow cytometry, it is shown that surface charge plays a pivotal role in both successful targeting and targeting strength, as quantified by MFI, by charged-based, nonaffinity binding. Highly specific targeting of the pulmonary microvasculature, an important target for therapy, was achieved using cationic polyplexes with a size and zeta potential near 120 d.nm and +24 mV in normal glucose, respectively, with a targeting percentage of 85–90 %. Live, whole body imaging further revealed the kidneys as possible secondary targets. Investigation

**Table 3.** Size and zeta potentials of PEI<sub>10k</sub>-LinA<sub>15</sub>-PEG<sub>3.0</sub> coated with 0%, 10%, 25%, and 50% PAA by mass.

	w/w = 4.5		w/w = 15		
	Z-average [d.nm]	Zeta potential [mV]	Z-average [d.nm]	Zeta potential [mV]	
PAA = 0%	120 ± 30	18.7 ± 5.1	PAA = 0%	105 ± 54	23.7 ± 7.4
PAA = 10%	184 ± 35	14.4 ± 4.2	PAA = 10%	443 ± 175	15.9 ± 3.2
PAA = 25%	126 ± 28	-17.4 ± 5.3	PAA = 25%	117 ± 40	-21.3 ± 6.0
PAA = 50%	107 ± 23	-24.2 ± 6.7	PAA = 50%	141 ± 83	-35.8 ± 7.7

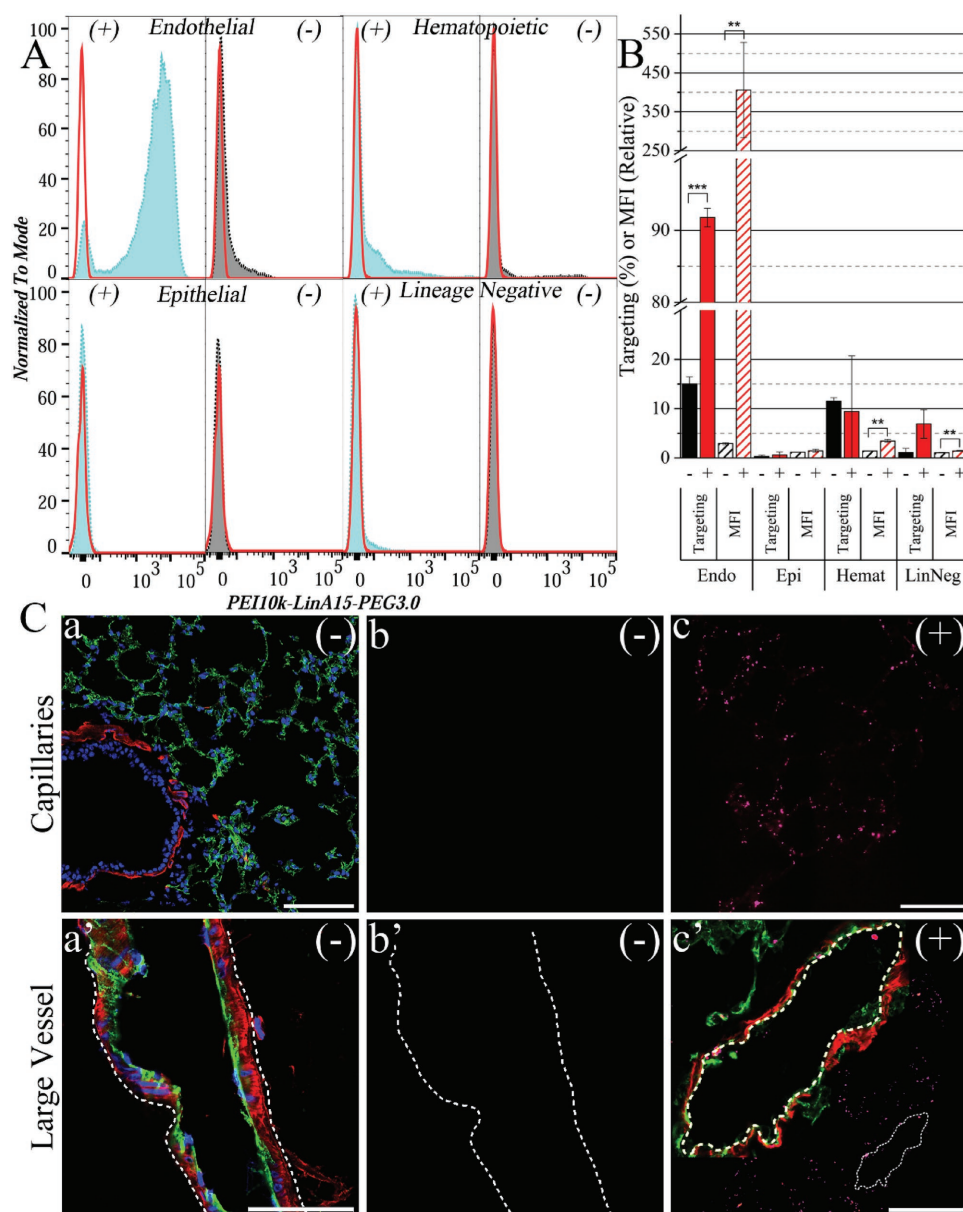


**Figure 5.** A) Targeting of PEI<sub>10k</sub>-LinA<sub>15</sub>-PEG<sub>3.0</sub> with positive (+) surface charge (blue filled) and negative (-) surface charge (black filled) against FMO controls (red line) within endothelial (Endo), hematopoietic (Hemat), epithelial (Epi), and lineage negative (LinNeg) populations. B) Quantification of targeting percentage (filled bars) and median fluorescent intensity (MFI, dashed bars) of (-) and (+) polyplexes within isolated populations (\*\*  $p < 0.01$ , \*\*\*  $p < 0.001$ ,  $n > 3$ ). C) Immunofluorescent images of lung microvasculature and large vessels for (-) and (+)-coated polyplexes. (C-b,b') nanoparticle only channel for (C-a,a') the respective field of view. (C-c,c') Nanoparticle only channel for (+) polyplexes showing (C-c) high affinity within microvasculature and (c') reduced targeting within large vessels. IF of (-) and (+) polyplexes are taken from different samples imaged under the same acquisition parameters. Scale bars: (C-a,c') 100  $\mu\text{m}$ ; (C-c,a') 50  $\mu\text{m}$ .

into the importance of surface charge was completed by charge switching using two anionic polymers, PAA and heparin, to establish a negative surface potential by two different functional groups. Percent targeting, MFI, and immunofluorescent staining of PAA- and heparin-coated polyplexes indicate that the major targeting mechanism within the lung of these highly efficient polyplexes derives from surface charge. It is therefore the combination of size and zeta potential, derived from the specific formulations of the polymeric nanoparticles, which has allowed for successful targeting and delivery nucleic acids to

the pulmonary microvascular network through selective charge-based binding in an uninjured mouse model.

## 5. Experimental Section

**Materials:** Methoxypolyethylene glycol amine  $M_n = 2000$  (PEG<sub>NH2</sub>) was obtained through Nanocs. *O*-Methyl-*O*'-succinylpolyethylene glycol  $M_n = 2000$ , polyethylenimine  $M_n = 600, 1800, 10k$  (PEI<sub>600</sub>, PEI<sub>1800</sub>, PEI<sub>10k</sub>), myristic acid ( $\geq 99\%$ ), LinA ( $\geq 99.0\%$ ), OA ( $\geq 99\%$ ), cholesterol (BioReagent,  $\geq 99\%$ ), ethanol (EtOH, 200p), high-performance liquid

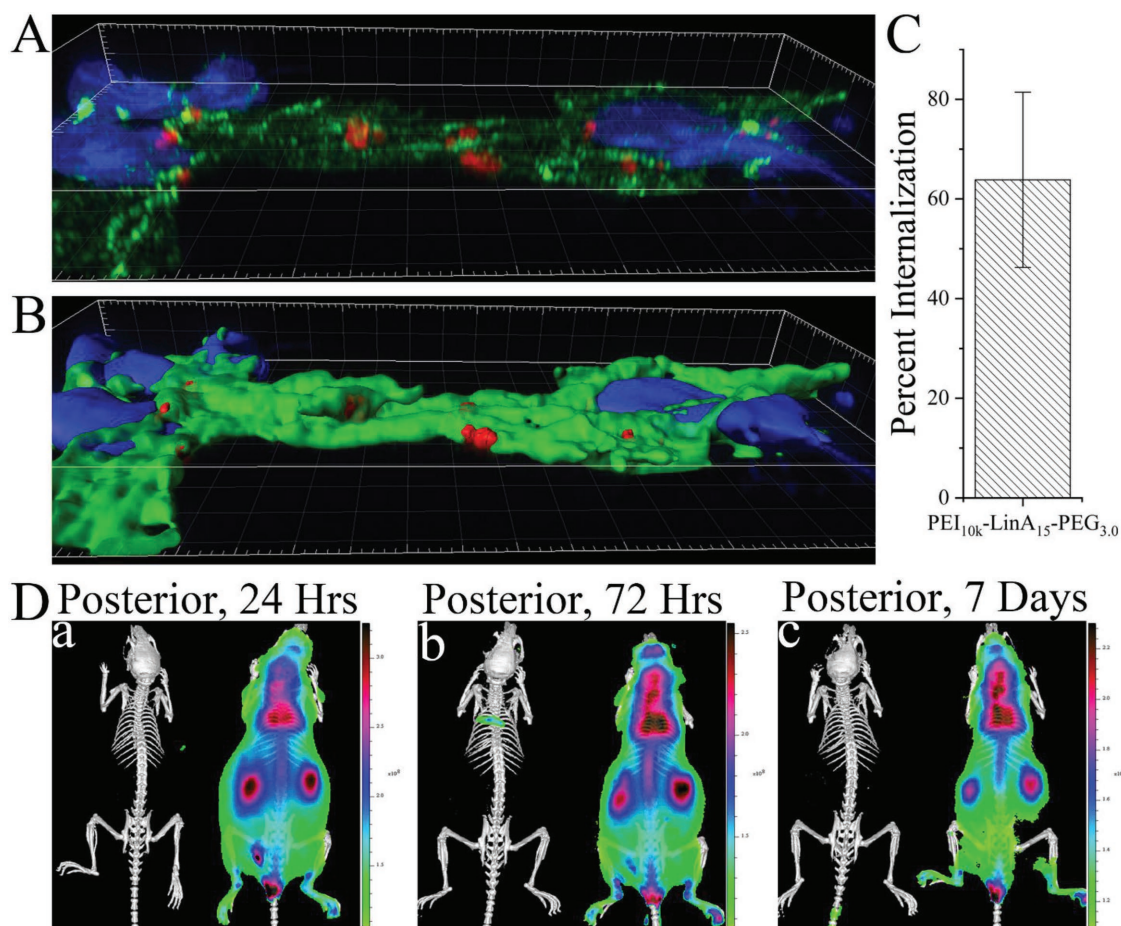


**Figure 6.** A) 3D deconvolution of PECAM1 (green) cells within the microvasculature showing colocalization with labeled PEI<sub>10k</sub>-LinA<sub>15</sub>-PEG<sub>3,0</sub> nanoparticles (red). B) Surface reconstruction from a maximum intensity projection shows nanoparticle fluorescence with subcellular and surface localizations. C) Percent internalization of nanoparticle fluorescence within PECAM1 cells calculated from the 3D deconvolution. D) IVIS live in vivo imaging of labeled PEI<sub>10k</sub>-LinA<sub>15</sub>-PEG<sub>3,0</sub> nanoparticles following I.V. injection at (D-a) 24 h, (D-b) 72 h, and (D-c) 7 days. Maximum fluorescence is found to be localized near the lungs and kidneys.

chromatography (HPLC) grade water, 2-(*N*-morpholino)ethanesulfonic acid (MES) ( $\geq 99\%$ ), 3-(*N*-morpholino)propanesulfonic acid (MOPS) were obtained through Sigma-Aldrich and used without further purification. EDC/NHS, and DyLight 650 NHS ester were obtained through ThermoFisher Scientific and used as received. Spectrum Spectra/Por 3.5 and 20 kDa molecular weight cutoff (MWCO) dialysis tubing were obtained through Fisher Scientific. Hoechst 33342 and ProLong Diamond were purchased from ThermoFisher. Stabilized eGFP RNA was obtained as a generous gift from TranscriptTX (Sunnyvale, CA) through Dr. James Bridges' lab at the Cincinnati Children's Hospital Medical Center (CCHMC).

autoMACS running buffer was obtained from Miltenyl Biotec. Fixable Viability Dye eF780 was obtained from eBioscience. Dulbecco's modified Eagle's medium (DMEM), L-glutamine (100 $\times$ ), and antibiotic-antimycotic (100 $\times$ ) were obtained through ThermoFisher Scientific.

**Materials—Antibodies (Ab):** Anti-mouse CD16/CD32 (eBioscience, clone 93), anti-mouse CD31-eF405 (eBioscience, clone 390), anti-mouse CD45-eVolve655 (eBioscience, clone 30-F11), anti-mouse CD326-PerCP-eF710 (eBioscience, clone G8.8), rat anti-mouse CD31 (BD Bioscience, clone MEC13.3), mouse anti-mouse  $\alpha$ SMA, donkey anti-rat AlexaFluor488 (ThermoFisher), donkey anti-mouse AlexaFluor594 (ThermoFisher).

**Materials—Buffers:** MES was dissolved into double distilled H<sub>2</sub>O to a concentration of  $500 \times 10^{-3}$  M. pH was adjusted to 6.0 with 5 N NaOH. MOPS was dissolved into double distilled H<sub>2</sub>O to a concentration

$100 \times 10^{-3}$  M. The pH was adjusted to 7.4 with 2 N NaOH and the buffer diluted to  $10 \times 10^{-3}$  M. Buffer solutions were then filtered through a  $0.22 \mu\text{m}$  filter.

**Conjugated Polymethylenimine:** Functionalization of PEI with biological fatty acids and PEG was completed through amidation using EDC/NHS-mediated coupling. A general reaction scheme was used for all coupling reactions. For PEI conjugation, the mass of EDC was based on the EDC:COOH molar ratio of 1.25:1 and the mass of NHS was based on the NHS:EDC molar ratio of 1.25:1. EDC:COOH and NHS:COOH ratios for PEG<sub>NH2</sub> conjugation were 1.25:1 and 2:1, respectively.  $500 \times 10^{-3}$  M MES buffer volume, pH = 6, was based upon the molar ratio of 30:1, H<sub>2</sub>O:COOH. Initially, EDC and NHS were solvated in EtOH with half the volume of MES buffer and allowed to react for 15 min. A predetermined amount of PEI was solvated in EtOH with the remaining volume of MES buffer. The total volume of EtOH was determined to be the volume required for a final concentration of 95% EtOH. A final concentration of 99% EtOH was used for PEG<sub>NH2</sub> conjugation. Solvated PEI was quickly added following carboxylate activation and the solution was allowed to react overnight at 40 °C. EtOH was removed by rotary evaporation following conjugation and the resulting product was resuspended in deionized H<sub>2</sub>O. Conjugated PEI was dialyzed against deionized H<sub>2</sub>O using a 20 kDa membrane for 4–5 days, extracted twice in diethyl ether, and lyophilized. Lyophilized polymers were suspended in  $10 \times 10^{-3}$  M MOPS, pH = 7.4 and sonicated prior to use using a cup horn sonicator. Cho was solvated into EtOH at a concentration

of 10 mg mL<sup>-1</sup>. Cho and PEG-OA were incorporated into PEI-MA<sub>5</sub> colloids through solvent diffusion and vigorous mixing by continuous vortexing during addition. Ethanol was removed by lyophilization under glucose as a cryoprotectant. Lyophilized polymer was resuspended in sterile, molecular biology grade water under sonication. Polymers were fluorescently tagged using NHS-functionalized fluorophores at a ratio of 12.5 μg of NHS-functionalized fluorophore to 1 mg of polymer in 10 × 10<sup>-3</sup> M MOPS buffer, pH = 7.4, and allowed to react overnight at room temperature in the dark.

**Gel Electrophoresis:** Tris/borate/ethylenediaminetetraacetic acid (TBE)-based agarose gels (0.8% w/v, 0.5× TBE) were used to examine the complexation ratios of DNA with PEI-based vectors. Cytomegalovirus driven (CMV)-plasmid DNA (1 μg) was incubated at varying mass ratios with PEI-based vectors. Complexation was allowed for 15 min before gel loading. Gels were run at 120 V and imaged on a Bio-Rad Gel Doc.

**Polyplex Formation:** For sizing and zeta-potential analysis, 10 μg of CMV-plasmid DNA was mixed with polymer formulations at various mass ratios in 100 μL normal glucose supplemented with 10 × 10<sup>-3</sup> M MOPS, pH = 7.4, at room temperature. Polyplexes were allowed to rest at room temperature at least 10 min before analysis. The surface potential of formulated cationic polyplexes was switched through coating with either PAA or heparin by charge association following this 10 min period. 20 mg mL<sup>-1</sup> stock solutions of PAA or heparin, buffered to 7.4, were quickly mixed with formulated polyplexes at set mass ratios relative to that of the cationic polymer and allowed to bind for at least 10 min before use. For *in vivo* delivery, 40 μg of CMV driven plasmids were mixed with PEI<sub>600</sub>-MA<sub>5</sub>/PEG-OA/Cho, PEI<sub>1800</sub>-LinA<sub>5</sub>-PEG<sub>0.3</sub>, and PEI<sub>10k</sub>-LinA<sub>15</sub>-PEG<sub>3.0</sub> at mass ratios of 21, 25, 15 w/w, respectively, in normal glucose. These mass ratios corresponded to 3×, 10×, and 10× the w/w ratio required to stabilize DNA as determined by gel electrophoresis. Negatively charged polyplexes for *in vivo* delivery were created by coating with either PAA at a 50% mass ratio or heparin at a 100% mass ratio as described above.

**In Vivo Flow Cytometry:** All animal experiments were carried out in accordance to CCHMC guidelines using approved animal protocols. Mice were given free access to food and water over the course of the study. For stabilized RNA injections, 30 μg of eGFP RNA was mixed with PEI<sub>10k</sub>-LinA<sub>15</sub>-PEG<sub>3.0</sub> at a mass ratio of 4.5. A final volume of 250 or 200 μL was used for tail vein injection of plasmids or RNA, respectively, into wild-type C57BL/6, 8–10 weeks of age. Whole lungs were harvested 24 h post I.V. injection. FACS analysis was performed using a BD Biosciences LSR II.

Lungs were digested using a lysis buffer of DMEM supplemented with L-glutamine, antibiotics/antimycotics, 0.5 mg mL<sup>-1</sup> DNase, 100 μg mL<sup>-1</sup> liberase. Cells were isolated from the extracellular matrix and blocked in MACS buffer with CD16/CD32 Abs. Cells were then stained with CD31 Ab labeled with eF40, CD45 Ab labeled with eVolve655, and CD326 Ab labeled with PerCP-eF710. Dead cells were stained with fixable viability dye—eF780 (FVD). Populations were gated on live singlets as CD31+ CD45– CD326– (endothelial), CD45+CD31–CD326– (hematopoietic), CD326+CD31–CD45– (epithelial), CD45– CD31– CD326– (lineage negative).

**Live Imaging:** 40 μg of CMV driven plasmids were mixed with PEI<sub>10k</sub>-LinA<sub>15</sub>-PEG<sub>3.0</sub> at a mass ratio of 15 w/w, respectively, in normal glucose. A final volume of 250 μL was used for tail vein injection into adult, nude mice. Mice were anesthetized under 3–5% isoflurane and maintained at 1–2% while imaging. Fluorescence was imaged using standard transillumination.

**Immunofluorescence:** Lungs from wild-type C57BL6/J mice (8–10 weeks old) were inflated with 1:1 phosphate-buffered saline (PBS):optimal cutting temperature (OCT) compound and frozen in OCT. 10 μm sections were fixed for 10 min at –20 °C in 1:1 methanol:acetone, washed in 0.3% Tween 20 in PBS, and blocked in 4% donkey serum/2% fetal bovine serum (FBS)/0.1% Tween 20 in PBS. The antibody buffer used during staining was 0.4% donkey serum/0.2% FBS/0.1% Tween 20 in phosphate-buffered saline/tween (PBST). Rat anti-CD31 and mouse anti-αSMA were diluted in buffer at 1:250 and 1:2000 dilutions, respectively, and incubated overnight at 4 °C. Slides were washed and

incubated with donkey anti-rat labeled with AF488 and donkey anti-mouse labeled with AF594 overnight at 4 °C. Slides were washed, stained with Hoechst 33342, and mounted with ProLong Diamond on #1.5 cover glass. Imaging was done using a Nikon A1 confocal microscope with Richardson–Lucy deconvolution in Nikon Elements and analysis performed in Imaris.

**Characterization:** Infrared spectroscopy was run on a Nicolet atr-FTIR spectrometer outfitted with a diamond crystal. NMR was taken in deuterated chloroform on a Bruker AV 400 MHz spectrometer. Hydrodynamic size and zeta potential were measured on a Malvern Zetasizer Nano ZS in normal glucose.

**Characterization—DoC:** Fatty acid and PEG conjugation onto PEI was calculated through <sup>1</sup>H NMR spectroscopy using the terminal methyl group of the conjugated fatty acid (a), the integrated peak from the PEI backbone (g), and the integrated peak from PEG (c). Myristic acid and linoleic acid gave rise to <sup>1</sup>H NMR peaks that overlapped with the PEI spectrum in (g). Therefore, the following calculation method was used to decouple the two signals where (P) is the relative integration of the PEI + fatty acid peak, (Z) is the relative integration of the terminal methyl peak, (B) is the number of hydrogens contributing to (P) relative to the terminal methyl group. For myristic and linoleic acid, B is equal to 2 and 4, respectively. (X) is the decoupled, relative PEI integration. (Y) is the decoupled, relative fatty acid integration, and (C) is the total number of hydrogens in the PEI backbone as estimated from molecular weight. For PEG conjugation, only Equations (1) and (3) were used; (Y) and (B) in Equation (3) were then equivalent to the relative PEG integration and the total number of hydrogens in the PEG backbone determined from molecular weight.

$$[P - Z \times (B/3)] = X \quad (1)$$

$$P - X = Y \quad (2)$$

$$\frac{C - DoC}{X} \times \frac{Y}{B} = DoC \quad (3)$$

**Characterization—Statistics:** Values were reported as mean ± 1σ. Significance was calculated using an unpaired Welch's *t*-test assuming unequal variance.

## Supporting Information

Supporting Information is available from the Wiley Online Library or from the author.

## Acknowledgements

The authors acknowledge support from the National Science Foundation grant CMMI-1635089 (to D.S.) and the NIH grants HL84151, HL123490, and HL141174 (to V.V.K.).

## Conflict of Interest

The authors declare no conflict of interest.

## Keywords

*in vivo* targeting, nanotechnology, polymer science

Received: July 24, 2018  
Revised: September 26, 2018  
Published online:

- [1] R. H. Steinhorn, *Pediatr. Crit. Care Med.* **2010**, *11*, S79.
- [2] H. Kool, D. Mous, D. Tibboel, A. Klein, R. J. Rottier, *Birth Defects Res., Part C* **2014**, *102*, 343.
- [3] P. M. Mourani, S. H. Abman, *Curr. Opin. Pediatr.* **2013**, *25*, 329.
- [4] P. M. Mourani, M. K. Sontag, A. Younoszai, J. I. Miller, J. P. Kinsella, C. D. Baker, B. B. Poindexter, D. A. Ingram, S. H. Abman, *Am. J. Respir. Crit. Care Med.* **2015**, *191*, 87.
- [5] L. Farkas, D. Farkas, K. Ask, A. Mller, J. Gauldie, P. Margetts, M. Inman, M. Kolb, *J. Clin. Invest.* **2009**, *119*, 1298.
- [6] Z. Cao, R. Lis, M. Ginsberg, D. Chavez, K. Shido, S. Y. Rabbany, G. Fong, T. P. Sakmar, S. Rafii, B. Ding, *Nat. Med.* **2016**, *22*, 154.
- [7] D. A. Muruve, M. J. Barnes, I. E. Stillman, T. A. Libermann, *Hum. Gene Ther.* **1999**, *10*, 965.
- [8] D. A. Muruve, *Hum. Gene Ther.* **2004**, *15*, 1157.
- [9] S. Nayak, R. W. Herzog, *Gene Ther.* **2010**, *17*, 295.
- [10] M. Neu, D. Fischer, T. Kissel, *J. Gene Med.* **2005**, *7*, 992.
- [11] A. K. Varkouhi, M. Scholte, G. Storm, H. J. Haisma, *J. Controlled Release* **2011**, *151*, 220.
- [12] W. T. Godbey, K. K. Wu, A. G. Mikos, *J. Biomed. Mater. Res.* **1999**, *45*, 268.
- [13] W. T. Godbey, K. K. Wu, A. G. Mikos, *J. Controlled Release* **1999**, *60*, 149.
- [14] U. Lungwitz, M. Breunig, T. Blunk, A. Gopferich, *Eur. J. Pharm. Biopharm.* **2005**, *60*, 247.
- [15] H. C. Kang, H. J. Kang, Y. H. Bae, *Biomaterials* **2011**, *32*, 1193.
- [16] A. Schroeder, J. E. Dahlman, G. Sahay, K. T. Love, S. Jiang, A. A. Eltoukhy, C. G. Levins, Y. Wang, D. G. Anderson, *J. Controlled Release* **2012**, *160*, 172.
- [17] O. F. Khan, E. W. Zaia, S. Jhunjunwala, W. Xue, W. Cai, D. S. Yun, C. M. Barnes, J. E. Dahlman, Y. Dong, J. M. Pelet, **2015**, *15*, 3008.
- [18] J. Dai, S. Zou, Y. Pei, D. Cheng, H. Ai, X. Shuai, *Biomaterials* **2011**, *32*, 1694.
- [19] M. Zheng, Y. Zhong, F. Meng, R. Peng, Z. Zhong, *Mol. Pharmaceutics* **2011**, *8*, 2434.
- [20] G. Navarro, S. Essex, R. R. Sawant, S. Biswas, D. Nagesha, S. Sridhar, C. T. de Ilarduya, V. P. Torchilin, *Nanomedicine* **2014**, *10*, 411.
- [21] J. Li, D. Cheng, T. Yin, W. Chen, Y. Lin, J. Chen, R. Li, X. Shuai, *Nanoscale* **2014**, *6*, 1732.
- [22] A. Masotti, F. Moretti, F. Mancini, G. Russo, N. Di Lauro, P. Checchia, C. Marianecchi, M. Carafa, E. Santucci, G. Ortaggi, *Bioorg. Med. Chem.* **2007**, *15*, 1504.
- [23] G. Guo, L. Zhou, Z. Chen, W. Chi, X. Yang, W. Wang, B. Zhang, *Int. J. Pharm.* **2013**, *450*, 44.
- [24] L. Liu, M. Zheng, T. Renette, T. Kissel, *Bioconjugate Chem.* **2012**, *23*, 1211.
- [25] A. Zintchenko, A. Philipp, A. Dehshahri, E. Wagner, *Bioconjugate Chem.* **2008**, *19*, 1448.
- [26] R. M. Schiffelers, A. Ansari, J. Xu, Q. Zhou, Q. Tang, G. Storm, G. Molema, P. Y. Lu, P. V. Scaria, M. C. Woodle, *Nucleic Acids Res.* **2004**, *32*, e149.
- [27] M. L. Forrest, J. T. Koerber, D. W. Pack, *Bioconjugate Chem.* **2003**, *14*, 934.
- [28] P. Y. Teo, C. Yang, J. L. Hedrick, A. C. Engler, D. J. Coady, S. Ghaem-Maghami, A. J. T. George, Y. Y. Yang, *Biomaterials* **2013**, *34*, 7971.
- [29] K. T. Love, K. P. Mahon, C. G. Levins, K. A. Whitehead, W. Querbes, J. R. Dorkin, J. Qin, W. Cantley, L. L. Qin, T. Racie, M. Frank-Kamenetsky, K. N. Yip, R. Alvarez, D. W. Sah, A. de Fougerolles, K. Fitzgerald, V. Koteliensky, A. Akinc, R. Langer, D. G. Anderson, *Proc. Natl. Acad. Sci. USA* **2010**, *107*, 1864.
- [30] Y. Dong, K. T. Love, J. R. Dorkin, S. Sirirungruang, Y. Zhang, D. Chen, R. L. Bogorad, H. Yin, Y. Chen, A. J. Vegas, *Proc. Natl. Acad. Sci. USA* **2014**, *111*, 3955.
- [31] G. T. Noble, J. F. Stefanick, J. D. Ashley, T. Kiziltepe, B. Bilgicer, *Trends Biotechnol.* **2014**, *32*, 32.
- [32] J. E. Dahlman, C. Barnes, O. F. Khan, A. Thiriort, S. Jhunjunwala, T. E. Shaw, Y. Xing, H. B. Sager, G. Sahay, L. Speciner, *Nat. Nanotechnol.* **2014**, *9*, 648.
- [33] R. Gref, M. Luck, P. Quellec, M. Marchand, E. Dellacherie, S. Harnisch, T. Blunk, R. H. Muller, *Colloids Surf., B* **2000**, *18*, 301.
- [34] C. Fang, B. Shi, Y. Y. Pei, M. H. Hong, J. Wu, H. Z. Chen, *Eur. J. Pharm. Sci.* **2006**, *27*, 27.
- [35] S. Essex, G. Navarro, P. Sabhachandani, A. Chordia, M. Trivedi, S. Movassaghian, V. P. Torchilin, *Gene Ther.* **2015**, *22*, 41.
- [36] I. A. Babar, C. J. Cheng, C. J. Booth, X. Liang, J. B. Weidhaas, W. M. Saltzman, F. J. Slack, *Proc. Natl. Acad. Sci. USA* **2012**, *109*, E1695.
- [37] E. Blanco, H. Shen, M. Ferrari, *Nat. Biotechnol.* **2015**, *33*, 941.
- [38] J. Han, Q. Wang, Z. Zhang, T. Gong, X. Sun, *Small* **2014**, *10*, 524.
- [39] A. E. Nel, L. Mädler, D. Velegol, T. Xia, E. M. Hoek, P. Somasundaran, F. Klaessig, V. Castranova, M. Thompson, *Nat. Mater.* **2009**, *8*, 543.
- [40] Z. Shriver, I. Capila, G. Venkataraman, R. Sasisekharan, in *Heparin - A Century of Progress* (Eds: R. Lever, B. Mulloy, C. P. Page), Springer, Berlin, Heidelberg **2012**, p. 159.
- [41] S. Reitsma, D. W. Slaaf, H. Vink, M. A. Van Zandvoort, M. G. Oude Egbrink, *Pflügers Arch.* **2007**, *454*, 345.
- [42] W. Jiang, B. Y. S. Kim, J. T. Rutka, W. C. W. Chan, *Nat. Nanotechnol.* **2008**, *3*, 145.
- [43] N. Oh, J. Park, *Int. J. Nanomed.* **2014**, *9*, 51.
- [44] Y. Wen, S. Pan, X. Luo, X. Zhang, W. Zhang, M. Feng, *Bioconjugate Chem.* **2009**, *20*, 322.
- [45] S. M. Danilov, V. D. Gavrilyuk, F. E. Franke, K. Pauls, D. W. Harshaw, T. D. McDonald, D. J. Miletich, V. R. Muzykantov, *Am. J. Physiol.: Lung Cell. Mol. Physiol.* **2001**, *208*, L1335.
- [46] J. Murciano, S. Muro, L. Koniaris, M. Christofidou-Solomidou, D. W. Harshaw, S. M. Albelda, D. N. Granger, D. B. Cines, V. R. Muzykantov, *Blood* **2003**, *101*, 3977.
- [47] B. Ding, C. Gottstein, A. Grunow, A. Kuo, K. Ganguly, S. M. Albelda, D. B. Cines, V. R. Muzykantov, *Blood* **2005**, *106*, 4191.
- [48] B. D. Kozower, M. Christofidou-Solomidou, T. D. Sweitzer, S. Muro, D. G. Buerk, C. C. Solomides, S. M. Albelda, G. A. Patterson, V. R. Muzykantov, *Nat. Biotechnol.* **2003**, *21*, 392.